Magneto-gyrotropic photogalvanic effects in semiconductor quantum wells

2005 J. Phys.: Condens. Matter 17 3405

(http://iopscience.iop.org/0953-8984/17/21/032)

INSTITUTE OF PHYSICS PUBLISHING JOURNAL OF PHYSICS: CONDENSED MATTER

J. Phys.: Condens. Matter **17** (2005) 3405–3428 doi:10.1088/0953-8984/17/21/032

Magneto-gyrotropic photogalvanic effects in semiconductor quantum wells

V V Bel'kov[1,2], S D Ganichev[1,2], E L Ivchenko[2], S A Tarasenko[2], W Weber[1], S Giglberger[1], M Olteanu[1], H-P Tranitz[1], S N Danilov[1], Petra Schneider[1], W Wegscheider[1], D Weiss[1] and W Prettl[1]

[1] Fakultät Physik, University of Regensburg, 93040, Regensburg, Germany
[2] A F Ioffe Physico-Technical Institute, Russian Academy of Sciences, 194021 St Petersburg, Russia

Received 26 January 2005
Published 13 May 2005
Online at stacks.iop.org/JPhysCM/17/3405

Abstract

We show that free-carrier (Drude) absorption of both polarized and unpolarized terahertz radiation in quantum well (QW) structures causes an electric photocurrent in the presence of an in-plane magnetic field. Experimental and theoretical analysis evidences that the observed photocurrents are spin dependent and related to the gyrotropy of the QWs. Microscopic models for the photogalvanic effects in QWs based on asymmetry of photoexcitation and relaxation processes are proposed. In most of the investigated structures the observed magneto-induced photocurrents are caused by spin-dependent relaxation of non-equilibrium carriers.

1. Introduction

Much current interest in condensed matter physics is directed towards understanding of spin-dependent phenomena. In particular, the spin of electrons and holes in solid state systems is the decisive ingredient for spintronic devices [1]. Recently, spin photocurrents generated in QWs and bulk materials have attracted considerable attention [2, 3]. Among them are currents caused by a gradient of a spin-polarized electron density [4–6], the spin-galvanic effect [7], the circular photogalvanic effect in QWs [8], pure spin currents under simultaneous one- and two-photon coherent excitation [9, 10] and spin-polarized currents due to the photovoltaic effect in p–n junctions [11]. Experimentally, a natural way to generate spin photocurrents is optical excitation with circularly polarized radiation. The absorption of circularly polarized light results in optical spin orientation of free carriers due to a transfer of photon angular momenta to the carriers [12]. Because of the spin–orbit coupling such excitation may result in an electric current. A characteristic feature of this electric current is that it reverses its direction upon changing the radiation helicity from left handed to right handed and vice versa.

However, in an external magnetic field spin photocurrents may be generated even by unpolarized radiation as has been proposed for bulk gyrotropic crystals [13, 14]. Here we report

on an observation of these spin photocurrents in QW structures caused by the Drude absorption of terahertz radiation. We show that, microscopically, the effects under study are related to the gyrotropic properties of the structures. The gyrotropic point group symmetry makes no difference between components of axial and polar vectors, and hence allows an electric current $j \propto I B$, where I is the light intensity and B is the applied magnetic field. Photocurrents which require simultaneously gyrotropy and the presence of a magnetic field may be gathered in a class of magneto-optical phenomena denoted as magneto-gyrotropic photogalvanic effects. So far such currents have been intensively studied in low-dimensional structures at direct interband and inter-subband transitions [15–22]. In these investigations the magneto-induced photocurrents were related to spin-independent mechanisms, except for [15, 20], where direct optical transitions between branches of the spin-split electron subband were considered. This mechanism requires, however, the spin splitting and the photon energy to be comparable, whereas in the conditions under study here the spin splitting is much smaller than the photon energy and the light absorption occurs due to indirect (Drude-like) optical transitions. It is clear that magneto-gyrotropic effects due to the Drude absorption may also be observed at excitation in the microwave range where the basic mechanism is free carrier absorption as well. This could link electronics to spin optics. In most of the investigated structures, the photogalvanic measurements reveal a magneto-induced current which is independent of the direction of light in-plane linear polarization and related to spin-dependent relaxation of non-equilibrium carriers. In addition, our results show that, without a magnetic field, non-equilibrium free carrier heating can be accompanied by spin flow similar to spin currents induced in experiments with simultaneous one- and two-photon coherent excitation [10] or in the spin Hall effect [23, 24].

2. Phenomenological theory

Illumination of gyrotropic nanostructures in the presence of a magnetic field may result in a photocurrent. There is a number of contributions to the magnetic-field-induced photogalvanic effect whose microscopic origins will be considered in section 5. The contributions are characterized by different dependences of the photocurrent magnitude and direction on the radiation polarization state and the orientation of the magnetic field with respect to the crystallographic axes. As a consequence, a proper choice of experimental geometry allows us to investigate each contribution separately. Generally, the dependence of the photocurrent on the light polarization and orientation of the magnetic field may be obtained from phenomenological theory which does not require knowledge of the microscopic origin of the current. Within the linear approximation in the magnetic field strength $\boldsymbol{B}$, the magneto-photogalvanic effect (MPGE) is given by

$$j_\alpha = \sum_{\beta\gamma\delta} \phi_{\alpha\beta\gamma\delta} B_\beta \{E_\gamma E_\delta^\star\} + \sum_{\beta\gamma} \mu_{\alpha\beta\gamma} B_\beta \hat{e}_\gamma E_0^2 P_{\mathrm{circ}}. \tag{1}$$

Here the fourth rank pseudo-tensor ϕ is symmetric in the last two indices; E_γ are components of the complex amplitude of the radiation electric field $\boldsymbol{E}$. In the following the field is presented as $E = E_0 \boldsymbol{e}$ with E_0 being the modulus $|\boldsymbol{E}|$ and $\boldsymbol{e}$ indicating the (complex) polarization unit vector, $|e| = 1$. The symbol $\{E_\gamma E_\delta^\star\}$ means the symmetrized product of the electric field with its complex conjugate,

$$\{E_\gamma E_\delta^\star\} = \tfrac{1}{2}\left(E_\gamma E_\delta^\star + E_\delta E_\gamma^\star\right). \tag{2}$$

In the second term on the right-hand side of equation (1), $\boldsymbol{\mu}$ is a regular third-rank tensor, P_{circ} is the helicity of the radiation and $\hat{e}$ is the unit vector pointing in the direction of light

Table 1. Definition of the parameters S_i and S'_i ($i = 1 \ldots 4$) in equations (3) in terms of non-zero components of the tensors ϕ and μ for the coordinates $x' \parallel [1\bar{1}0]$, $y' \parallel [110]$ and $z \parallel [001]$. The C_{2v} symmetry and normal incidence of radiation along z are assumed.

$S_1 = \frac{1}{2}(\phi_{x'y'x'x'} + \phi_{x'y'y'y'})$	$S'_1 = \frac{1}{2}(\phi_{y'x'x'x'} + \phi_{y'x'y'y'})$
$S_2 = \frac{1}{2}(\phi_{x'y'x'x'} - \phi_{x'y'y'y'})$	$S'_2 = \frac{1}{2}(\phi_{y'x'x'x'} - \phi_{y'x'y'y'})$
$S_3 = \phi_{x'x'x'y'} = \phi_{x'x'y'x'}$	$S'_3 = \phi_{y'y'x'y'} = \phi_{y'y'y'x'}$
$S_4 = \mu_{x'x'z}$	$S'_4 = \mu_{y'y'z}$

propagation. While the second term requires circularly polarized radiation, the first term may be non-zero even for unpolarized radiation.

We consider (001)-oriented QWs based on zinc-blende-lattice III–V or II–VI compounds. Depending on the equivalence or non-equivalence of the QW interfaces their symmetry may belong to one of the point groups D_{2d} or C_{2v}, respectively. The present experiments have been carried out on the C_{2v} symmetry structures and, therefore, here we will focus on these only.

For the C_{2v} point group, it is convenient to write the components of the magneto-photocurrent in the coordinate system with $x' \parallel [1\bar{1}0]$ and $y' \parallel [110]$ or in the system $x \parallel [100]$ and $y \parallel [010]$. The advantage of the former system is that the in-plane axes x', y' lie in the crystallographic planes (110) and $(1\bar{1}0)$ which are the mirror reflection planes containing the twofold axis C_2. In the system x', y', z for normal incidence of the light and the in-plane magnetic field, equation (1) is reduced to

$$\begin{aligned} j_{x'} &= S_1 B_{y'} I + S_2 B_{y'} \left(|e_{x'}|^2 - |e_{y'}|^2\right) I + S_3 B_{x'} \left(e_{x'} e^*_{y'} + e_{y'} e^*_{x'}\right) I + S_4 B_{x'} I P_{\mathrm{circ}}, \\ j_{y'} &= S'_1 B_{x'} I + S'_2 B_{x'} \left(|e_{x'}|^2 - |e_{y'}|^2\right) I + S'_3 B_{y'} \left(e_{x'} e^*_{y'} + e_{y'} e^*_{x'}\right) I + S'_4 B_{y'} I P_{\mathrm{circ}}, \end{aligned} \tag{3}$$

where, for simplicity, we set for the intensity $I = E_0^2$. The parameters S_1 to S_4 and S'_1 to S'_4 expressed in terms of non-zero components of the tensors ϕ and μ allowed by the C_{2v} point group are given in table 1. The first terms on the right-hand side of equation (3) (described by S_1, S'_1) yield a current in the QW plane which is independent of the radiation polarization. This current is induced even by unpolarized radiation. Each following contribution has a special polarization dependence which permits us to separate it experimentally from the others.

Linearly polarized radiation. For *linearly* polarized light, the terms described by parameters S_2, S'_2 and S_3, S'_3 are proportional to $|e_{x'}|^2 - |e_{y'}|^2 = \cos 2\alpha$ and $e_{x'} e^*_{y'} + e_{y'} e^*_{x'} = \sin 2\alpha$, respectively, where α is the angle between the plane of linear polarization and the x' axis. Hence the current reaches maximum values for light polarized either along x' or y' for the second terms (parameters S_2, S'_2), or along the bisector of x', y' for the third terms, proportional to S_3, S'_3. The last terms (parameters S_4, S'_4), being proportional to P_{circ}, vanish for *linearly* polarized excitation.

Elliptically polarized radiation. For *elliptically* polarized light all contributions are allowed. In the experiments discussed below, elliptically and, in particular, circularly polarized radiation was achieved by passing laser radiation, initially linearly polarized along the x' axis, through a $\lambda/4$-plate. Rotation of the plate results in a variation of both linear polarization and helicity as follows:

$$P_{\mathrm{lin}} \equiv \tfrac{1}{2}(e_{x'} e^*_{y'} + e_{y'} e^*_{x'}) = \tfrac{1}{4} \sin 4\varphi, \tag{4}$$

$$P'_{\mathrm{lin}} \equiv \tfrac{1}{2}(|e_{x'}|^2 - |e_{y'}|^2) = \frac{1 + \cos 4\varphi}{4}, \tag{5}$$

$$P_{\mathrm{circ}} = \sin 2\varphi. \tag{6}$$

Two Stokes parameters, P_{lin} and P'_{lin}, describe the degrees of linear polarization, and φ is the angle between the optical axis of the $\lambda/4$ plate and the direction of the initial polarization x'.

Table 2. Definition of the parameters S_i^+ and S_i^- ($i = 1 \ldots 4$) in equations (7) in terms of non-zero components of the tensors ϕ and μ for the coordinates $x \parallel [100]$, $y \parallel [010]$ and $z \parallel [001]$. The C_{2v} symmetry and normal incidence of radiation along z are assumed.

$S_1^+ = \frac{1}{2}(\phi_{xxxx} + \phi_{xxyy})$	$S_1^- = \frac{1}{2}(\phi_{xyxx} + \phi_{xyyy})$
$= -\frac{1}{2}(\phi_{yyxx} + \phi_{yyyy})$	$= -\frac{1}{2}(\phi_{yxxx} + \phi_{yxyy})$
$S_2^+ = \phi_{yyxy} = \phi_{yyyx}$	$S_2^- = \phi_{yxxy} = \phi_{yxyx}$
$= -\phi_{xxxy} = -\phi_{xxyx}$	$= -\phi_{xyxy} = -\phi_{xyyx}$
$S_3^+ = \frac{1}{2}(\phi_{xxxx} - \phi_{xxyy})$	$S_3^- = -\frac{1}{2}(\phi_{xyxx} - \phi_{xyyy})$
$= \frac{1}{2}(\phi_{yyxx} - \phi_{yyyy})$	$= -\frac{1}{2}(\phi_{yxxx} - \phi_{yxyy})$
$S_4^+ = \mu_{xxz} = \mu_{yyz}$	$S_4^- = -\mu_{xyz} = -\mu_{yxz}$

As described above, the first terms on the right-hand side of equation (3) are independent of the radiation polarization. The polarization dependences of magneto-induced photocurrents caused by second and third terms in equation (3) are proportional to $P'_{\rm lin}$ and $P_{\rm lin}$, respectively. These terms vanish if the radiation is circularly polarized. In contrast, the last terms in equation (3) describe a photocurrent proportional to the helicity of radiation. It is zero for linearly polarized radiation and reaches its maximum for left- or right-handed circular polarization. Switching helicity $P_{\rm circ}$ from +1 to −1 reverses the current direction.

As we will see below, the photocurrent analysis for $x \parallel [100]$ and $y \parallel [010]$ directions helps to conclude on the microscopic nature of the different contributions to the MPGE. In these axes equations (3) read

$$
\begin{aligned}
j_x = {} & S_1^+ B_x I + S_1^- B_y I - (S_2^+ B_x + S_2^- B_y)\left(e_x e_y^* + e_y e_x^*\right) I \\
& + (S_3^+ B_x - S_3^- B_y)\left(|e_x|^2 - |e_y|^2\right) I + (S_4^+ B_x - S_4^- B_y) I P_{\rm circ}, \\
j_y = {} & -S_1^- B_x I - S_1^+ B_y I + (S_2^- B_x + S_2^+ B_y)\left(e_x e_y^* + e_y e_x^*\right) I \\
& + (-S_3^- B_x + S_3^+ B_y)\left(|e_x|^2 - |e_y|^2\right) I + (-S_4^- B_x + S_4^+ B_y) I P_{\rm circ},
\end{aligned}
\tag{7}
$$

where $S_l^\pm = (S_l \pm S'_l)/2$ ($l = 1 \ldots 4$). The parameters $S_1^\pm$ to $S_4^\pm$ expressed via non-zero elements of the tensors ϕ and μ for the C_{2v} symmetry are given in table 2. Equations (7) show that, for a magnetic field oriented along a cubic axis, all eight parameters $S_l^\pm$ contribute to the photocurrent components, either normal or parallel to the magnetic field. However, as well as for the magnetic field oriented along x' or y', the partial contributions can be separated analysing polarization dependences.

For the sake of completeness, in appendices A and B we present the phenomenological equations for the magneto-photocurrents in the systems of the T_d and $C_{\infty v}$ symmetries, respectively, representing the bulk zinc-blende-lattice semiconductors and axially symmetric QWs with non-equivalent interfaces.

Summarizing the macroscopic picture we note that, for normal incidence of the radiation on a (001)-grown QW, a magnetic field applied in the interface plane is required to obtain a photocurrent. In table 3 we present the relations between the photocurrent direction, the state of light polarization and the magnetic field orientation which follow from equations (3) and (7) and determine the appropriate experimental geometries (section 4). In order to ease data analysis we give in table 4 polarization dependences for geometries relevant to experiment. The specific polarization behaviour of each term allows us to discriminate between different terms in equations (3).

Table 3. Contribution of the different terms in equations (3) and equations (7) to the current at different magnetic field orientations. The two left columns indicate the magnetic field orientation and the photocurrent component, respectively.

		1st term	2nd term	3rd term	4th term
$B \parallel x'$	$j_{x'}/I$	0	0	$S_3 B_{x'}(e_{x'}e^*_{y'} + e_{y'}e^*_{x'})$	$S_4 B_{x'} P_{\rm circ}$
	$j_{y'}/I$	$S'_1 B_{x'}$	$S'_2 B_{x'}(\lvert e_{x'}\rvert^2 - \lvert e_{y'}\rvert^2)$	0	0
$B \parallel y'$	$j_{x'}/I$	$S_1 B_{y'}$	$S_2 B_{y'}(\lvert e_{x'}\rvert^2 - \lvert e_{y'}\rvert^2)$	0	0
	$j_{y'}/I$	0	0	$S'_3 B_{y'}(e_{x'}e^*_{y'} + e_{y'}e^*_{x'})$	$S'_4 B_{y'} P_{\rm circ}$
$B \parallel x$	j_x/I	$S_1^+ B_x$	$-S_2^+ B_x(e_x e^*_y + e_y e^*_x)$	$S_3^+ B_x(\lvert e_x\rvert^2 - \lvert e_y\rvert^2)$	$S_4^+ B_x P_{\rm circ}$
	j_y/I	$-S_1^- B_x$	$S_2^- B_x(e_x e^*_y + e_y e^*_x)$	$-S_3^- B_x(\lvert e_x\rvert^2 - \lvert e_y\rvert^2)$	$-S_4^- B_x P_{\rm circ}$
$B \parallel y$	j_x/I	$S_1^- B_y$	$-S_2^- B_y(e_x e^*_y + e_y e^*_x)$	$-S_3^- B_y(\lvert e_x\rvert^2 - \lvert e_y\rvert^2)$	$-S_4^- B_y P_{\rm circ}$
	j_y/I	$-S_1^+ B_y$	$S_2^+ B_y(e_x e^*_y + e_y e^*_x)$	$S_3^+ B_y(\lvert e_x\rvert^2 - \lvert e_y\rvert^2)$	$S_4^+ B_y P_{\rm circ}$

Table 4. Polarization dependences of different terms in equations (3) at $\boldsymbol{B} \parallel y'$.

		1st term	2nd term	3rd term	4th term
$j \parallel x'$	$j_{x'}(\varphi)$	$S_1 I B_{y'}$	$S_2 I B_{y'}(1 + \cos 4\varphi)/2$	0	0
	$j_{x'}(\alpha)$	$S_1 I B_{y'}$	$S_2 I B_{y'} \cos 2\alpha$	0	0
$j \parallel y'$	$j_{y'}(\varphi)$	0	0	$S'_3 I B_{y'}(\sin 4\varphi)/2$	$S'_4 I B_{y'} \sin 2\varphi$
	$j_{y'}(\alpha)$	0	0	$S'_3 I B_{y'} \sin 2\alpha$	0

Table 5. Parameters for non-illuminated samples at $T = 4.2$ K.

	Structure	Mobility ($\rm cm^2\ V^{-1}\ s^{-1}$)	Electron density ($\rm cm^{-2}$)
A1	(001)-InAs single QW of 15 nm width	$\approx 3 \times 10^5$	8×10^{11}
A2	(001)-GaAs double QW of 9.0 and 10.8 nm width	1.4×10^5	1.12×10^{11}
A3	(001)-GaAs heterojunction	3.53×10^6	1.08×10^{11}
A4	(001)-GaAs heterojunction	3.5×10^6	1.1×10^{11}
A5	(001)-GaAs multiple QW (30 QWs of 8.2 nm width)	2.57×10^4	9.3×10^{11}

3. Methods

The experiments were carried out on MBE-grown (001)-oriented n-type GaAs/$Al_{0.3}Ga_{0.7}As$ and InAs/AlGaSb QW structures. The characteristics of the investigated samples are given in table 5. The InAs/AlGaSb heterostructure was grown on a semi-insulating GaAs substrate. The quantum well is nominally undoped, but contains a two-dimensional electron gas with the carrier density of 8×10^{11} $\rm cm^{-2}$ at 4.2 K located in the InAs channel. Details of the growth procedure are given in [25]. All GaAs samples are modulation doped. For samples A2–A4 Si-δ-doping, either one sided with spacer layer thicknesses of 70 nm (A3) and 80 nm (A4), or double sided with 70 nm spacer layer thickness (A2), has been used. In contrast, for sample A5 the AlGaAs barrier layer separating the QWs has been homogeneously Si doped on a length of 30 nm. In the sample with a QW separation of 40 nm, this results in a spacer thickness of only 5 nm. Therefore, in addition to the different impurity distribution compared to samples A2–A4, sample A5 has much lower mobility.

All samples have two pairs of Ohmic contacts at the corners corresponding to the $x \parallel [100]$ and $y \parallel [010]$ directions, and two additional pairs of contacts centred at opposite sample edges

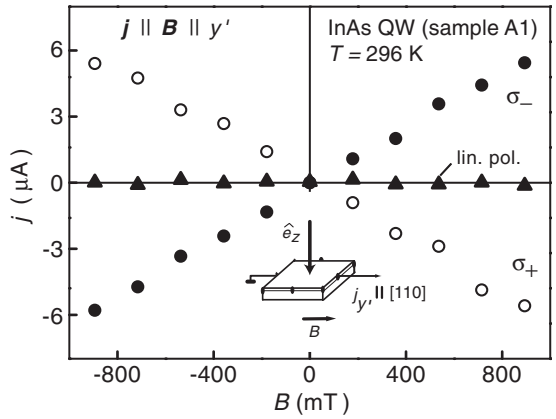

Figure 1. Magnetic field dependence of the photocurrent measured in sample A1 at room temperature with the magnetic field $\boldsymbol{B}$ parallel to the y' direction. Normally incident optical excitation of $P \approx 4$ kW is performed at wavelength $\lambda = 148$ μm with *linear* ($\boldsymbol{E} \parallel x'$), right-handed *circular* (σ_+) and left-handed *circular* (σ_-) polarization. The measured current component is *parallel* to $\boldsymbol{B}$. The inset shows the experimental geometry.

with the connecting lines along $x' \parallel [1\bar{1}0]$ and $y' \parallel [110]$ (see the inset in figure 1). The external magnetic field B up to 1 T was applied parallel to the interface plane.

A pulsed optically pumped terahertz laser was used for optical excitation [26]. With NH_3 as active gas 100 ns pulses of linearly polarized radiation with ∼10 kW power have been obtained at wavelengths of 148 and 90 μm. The terahertz radiation induces free carrier absorption in the lowest conduction subband e1 because the photon energy is smaller than the subband separation and much larger than the $\boldsymbol{k}$-linear spin splitting. The samples were irradiated along the growth direction.

In order to vary the angle between the polarization vector of the linearly polarized light and the magnetic field we placed a metal mesh polarizer behind a crystalline quartz $\lambda/4$-plate. After passing through the $\lambda/4$-plate initially linearly polarized laser light became circularly polarized. Rotation of the metal grid enabled us to obtain linearly polarized radiation with angle $\alpha = 0°$–$360°$ between the x' axis and the plane of linear polarization of the light incident upon the sample.

To obtain elliptically and, in particular, circularly polarized radiation the mesh polarizer behind the quartz $\lambda/4$-plate was removed. The helicity P_{circ} of the incident light was varied by rotating the $\lambda/4$-plate according to $P_{\mathrm{circ}} = \sin 2\varphi$ as given by equation (6). For $\varphi = n\pi/2$ with integer n the radiation was linearly polarized. Circular polarization was achieved with $\varphi = (2n + 1)(\pi/4)$, where even values of n including $n = 0$ yield the right-handed circular polarization σ_+ and odd n give the left-handed circular polarization σ_-.

The photocurrent $\boldsymbol{j}$ was measured at room temperature in unbiased structures via the voltage drop across a 50 Ω load resistor in closed circuit configuration. The voltage was measured with a storage oscilloscope. The measured current pulses of 100 ns duration reflected the corresponding laser pulses.

4. Experimental results

As follows from equations (3), the most suitable experimental arrangement for independent investigation of different contributions to the magneto-induced photogalvanic effect is achieved

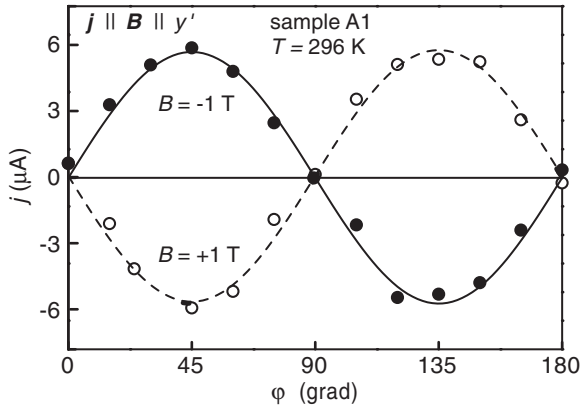

Figure 2. Photocurrent as a function of the phase angle φ defining the helicity. The photocurrent signal is measured in sample A1 at room temperature in the configuration $j \parallel B \parallel y'$ for two opposite directions of the magnetic field under normal incidence of the radiation with $\lambda = 148$ μm ($P \approx 4$ kW). The broken and full lines are fitted after equation (6).

by applying magnetic field along one of the crystallographic axes $x' \parallel [1\bar{1}0]$, $y' \parallel [110]$ and measuring the in-plane current along or normal to the magnetic field direction. Then, currents flowing perpendicular to the magnetic field contain contributions proportional only to the parameters S_1 and S_2 if $\boldsymbol{B} \parallel y'$ (or S_1' and S_2' if $\boldsymbol{B} \parallel x'$), whereas currents flowing parallel to the magnetic field arise only from terms proportional to S_3 and S_4 (or S_3' and S_4'). Further separation of contributions may be obtained by making use of the difference in their polarization dependences. The results obtained for $\lambda = 90$ and 148 μm are qualitatively the same. Therefore, we present only data obtained for $\lambda = 148$ μm.

4.1. Photocurrent parallel to the magnetic field ($\boldsymbol{j} \parallel \boldsymbol{B} \parallel y' \parallel [110]$)

According to equations (3) and table 4 only two contributions proportional to S_3' and S_4' are allowed in this configuration. While the S_3' contribution results in a current for linear or elliptical polarization, the S_4' one vanishes for linear polarization and assumes its maximum at circular polarization.

Irradiation of samples A1–A4 subjected to an in-plane magnetic field with normally incident *linearly* polarized radiation causes no photocurrent. However, *elliptically* polarized light yields a helicity-dependent current. Typical magnetic field and helicity dependences of this current are shown in figures 1 and 2. The polarity of the current changes upon reversal of the applied magnetic field as well as upon changing the helicity from right to left handed. The polarization behaviour of the current is well described by $j_{y'} \propto I B_{y'} P_{\mathrm{circ}}$. This means that the current is dominated by the last term on the right-hand side of the second equation (3) (parameter S_4') while the third term is vanishingly small. Observation of a photocurrent proportional to P_{circ} has already been reported previously. This is the spin-galvanic effect [7]. The effect is caused by the optical orientation of carriers, subsequent Larmor precession of the oriented electronic spins and asymmetric spin relaxation processes. Though, in general, the spin-galvanic current does not require an application of magnetic field, it may be considered as a magneto-photogalvanic effect under the above experimental conditions.

One of our QW structures, sample A5, showed a quite different behaviour. In this sample the dependence of the magneto-induced photocurrent on φ is well described by $j_{y'} \propto I B_{y'} \sin 4\varphi$ (see figure 3). In contrast to samples A1–A4, in sample A5 the spin-galvanic effect is overweighed by the contribution of the third term in equations (3). The latter should also appear under excitation with linearly polarized radiation. Figure 4 shows the dependence of the photocurrent on the angle α for one direction of the magnetic field. The current $j_{y'}$ is proportional to $I B_{y'} \sin 2\alpha$ as expected for the third term in equations (3).

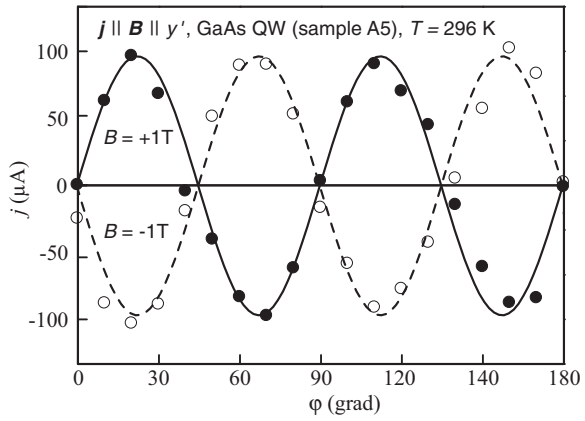

Figure 3. Photocurrent in sample A5 as a function of the phase angle φ defining the helicity for magnetic fields of two opposite directions. The photocurrent excited by normally incident radiation of $\lambda = 148$ μm ($P \approx 17$ kW) is measured at room temperature, $\boldsymbol{j} \parallel \boldsymbol{B} \parallel y'$. The broken and full lines are fitted after equation (4).

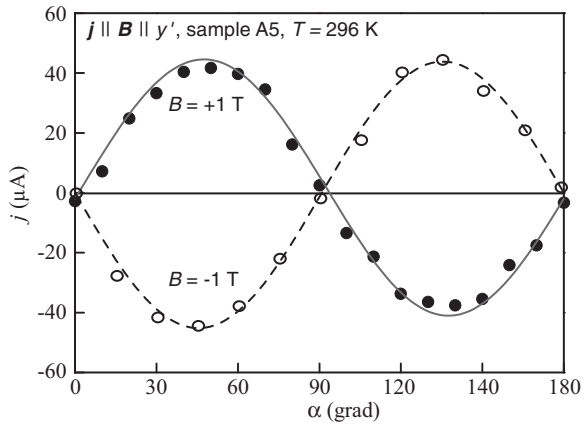

Figure 4. Photocurrent in sample A5 as a function of the azimuth angle α. The photocurrent $\boldsymbol{j} \parallel \boldsymbol{B} \parallel y'$ excited by normally incident *linearly* polarized radiation of $\lambda = 148$ μm ($P \approx 17$ kW) and measured at room temperature. The broken and full lines are fitted according to table 4, third term.

4.2. Current perpendicular to the magnetic field ($\boldsymbol{j} \perp \boldsymbol{B} \parallel y' \parallel [110]$)

In the transverse geometry only contributions proportional to the parameters S_1 and S_2 are allowed. Here samples A1–A4 and A5 again show different behaviour.

The data of a magnetic-field-induced photocurrent perpendicular to $\boldsymbol{B}$ in samples A1–A4 are illustrated in figure 5. The magnetic field dependence for sample A1 is shown for three different polarization states. Neither rotation of the polarization plane of the linearly polarized radiation nor variation of helicity changes the signal magnitude. Thus we conclude that the current strength and sign are independent of polarization. On the other hand, the current changes its direction upon the magnetic field reversal. This behaviour is described by $j_{x'} \propto I B_{y'}$ and corresponds to the first term on the right-hand side of the first equation in equations (3). The absence of a φ-dependence indicates that the second term in equations (3) is negligibly small. Note that the dominant contribution to the polarization-independent magneto-photogalvanic effect, described by the first term on the right side of equations (3), is observed for the same set of samples (A1–A4) where the longitudinal photocurrent is caused by the spin-galvanic effect.

In sample A5 a clear polarization dependence, characteristic for the second terms in equations (3), has been detected. The magnetic field and the polarization dependences obtained from this sample are shown in figures 6, 7 and 8, respectively. For sample A5 the φ-dependence

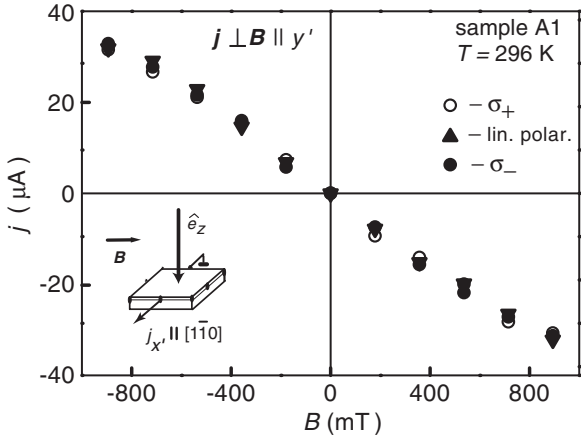

Figure 5. Magnetic field dependence of the photocurrent measured in sample A1 at room temperature with the magnetic field $\boldsymbol{B}$ parallel to the y' axis. Data are given for normally incident optical excitation of $P \approx 4$ kW at the wavelength $\lambda = 148$ μm for *linear* ($\boldsymbol{E} \parallel x'$), right-handed *circular* (σ_+) and left-handed *circular* (σ_-) polarization. The current is measured in the direction *perpendicular* to $\boldsymbol{B}$.

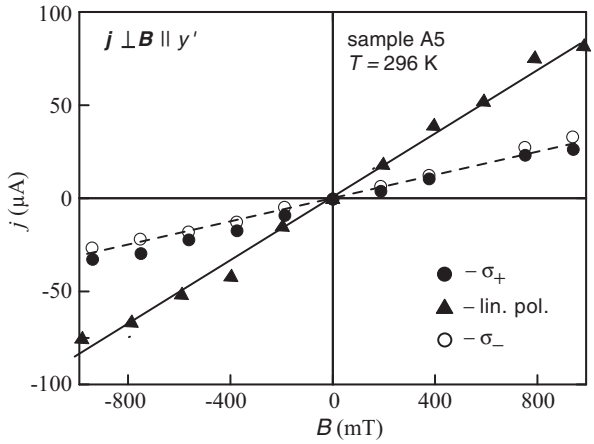

Figure 6. Magnetic field dependence of the photocurrent measured in sample A5 at room temperature with the magnetic field $\boldsymbol{B}$ parallel to the y' axis. Data are presented for normally incident optical excitation $P \approx 17$ kW at the wavelength $\lambda = 148$ μm for the *linear* ($\boldsymbol{E} \parallel x'$), right-handed *circular* (σ_+) and left-handed *circular* (σ_-) polarization. The current is measured in the direction *perpendicular* to $\boldsymbol{B}$.

can be well fitted by $S_1 + S_2(1+\cos 4\varphi)/2$ while the α-dependence is $S_1 + S_2 \cos 2\alpha$, as expected for the first and second terms in equations (3).

4.3. Magnetic field applied along the $x' \parallel [1\bar{1}0]$ direction

Rotation of $\boldsymbol{B}$ by 90° with respect to the previous geometry interchanges the role of the axes x' and y'. Now the magnetic field is applied along the $[1\bar{1}0]$ crystallographic direction. The magnetic field and polarization dependences observed experimentally in both configurations

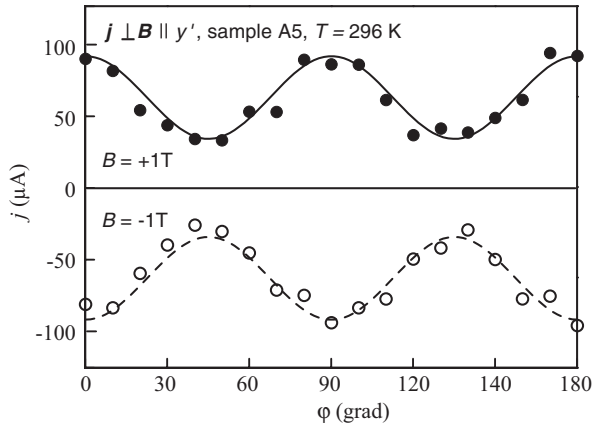

Figure 7. Photocurrent in sample A5 as a function of the phase angle φ defining the Stokes parameters; see equations (5). The photocurrent excited by normally incident radiation of $\lambda = 148$ μm ($P \approx 17$ kW) is measured at room temperature, $\boldsymbol{j} \perp \boldsymbol{B} \parallel y'$. The full and broken lines are fitted according to table 4, first and second terms.

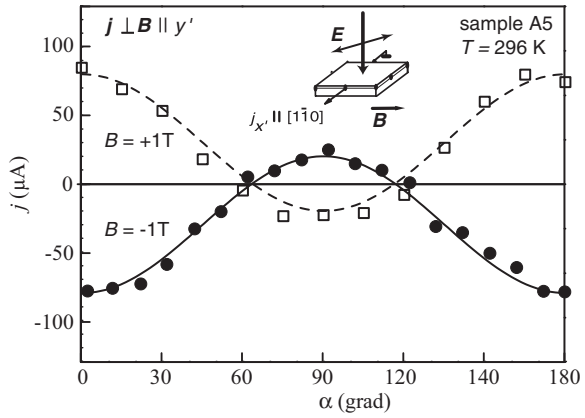

Figure 8. Photocurrent in sample A5 for $\boldsymbol{j} \perp \boldsymbol{B} \parallel y'$ as a function of the azimuth angle α. The photocurrent excited by normally incident radiation of $\lambda = 148$ μm ($P \approx 17$ kW) is measured at room temperature for magnetic fields of two opposite directions. The broken and full lines are fitted according to table 4, first and second terms.

are qualitatively similar. The only difference is the magnitude of the photocurrent. The observed difference in photocurrents is expected for C_{2v} point symmetry of the QW where the axes $[1\bar{1}0]$ and [110] are non-equivalent. This is taken into account in equations (3) by introducing independent parameters S_i and S_i' ($i = 1 \ldots 4$).

4.4. Magnetic field applied along the crystallographic axis x ∥ [100]

Under application of $\boldsymbol{B}$ along one of the in-plane cubic axes in a (001)-grown structure, all contributions to the photocurrent are allowed. This can be seen from equations (7) and table 3. In all samples both longitudinal and transverse currents are observed for *linearly* (figure 9) as well as *circularly* (figure 10) polarized excitation. In the absence of the magnetic field the current signals vanish for all directions. For samples A1–A4 a clear spin-galvanic current proportional to helicity P_{circ} and superimposed on a helicity-independent contribution is detected (see figure 10). The possibility of extracting the spin-galvanic effect is of particular importance in experiments aimed at the separation of Rashba- and Dresselhaus-like contributions to the spin–orbit interaction as has been recently reported [27].

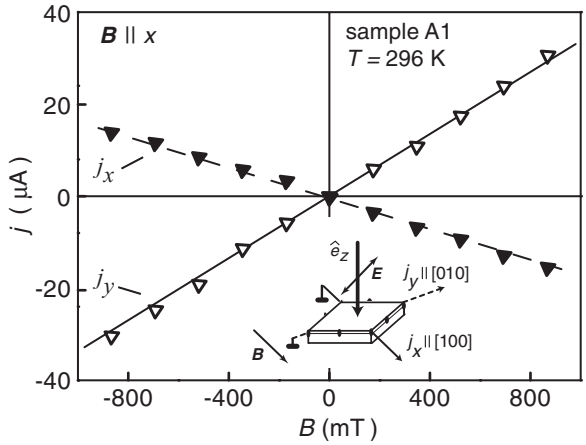

Figure 9. Magnetic field dependence of the photocurrent measured in sample A1 with the magnetic field $\boldsymbol{B}$ parallel to the [100] axis under photoexcitation with normally incident light of the wavelength $\lambda = 148$ μm ($P \approx 4$ kW) for *linear* polarization $\boldsymbol{E} \parallel y$. The current is measured in the directions *parallel* (j_x) and *perpendicular* (j_y) to $\boldsymbol{B}$.

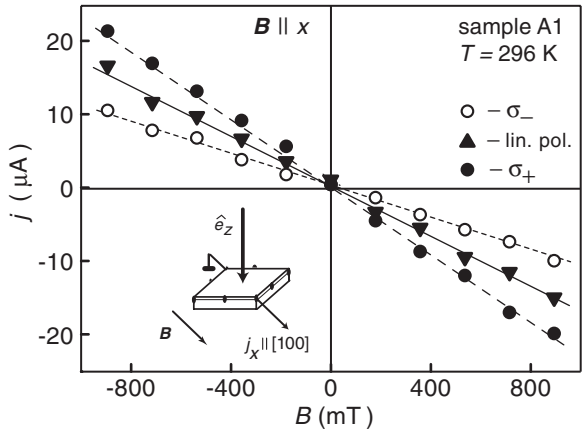

Figure 10. Magnetic field dependence of the photocurrent measured in sample A1 with the magnetic field $\boldsymbol{B}$ parallel to the [100] axis. Optical excitation of $P \approx 4$ kW at normal incidence was applied at wavelength $\lambda = 148$ μm for *linear* ($\boldsymbol{E} \parallel y$), right-handed *circular* (σ_+) and left-handed *circular* (σ_-) polarization. The current is measured in the direction *parallel* to $\boldsymbol{B}$.

5. Microscopic models

The term magneto-photogalvanic effects (MPGEs) stands for the generation of magnetic-field-induced photocurrent under polarized or unpolarized optical excitation. In this section we give a survey of possible microscopic mechanisms leading to MPGEs. Besides mechanisms discussed in the literature we also present here novel mechanisms. We start by recalling non-gyrotropic spin-independent mechanisms used to interpret MPGEs observed in bulk non-centrosymmetric semiconductors (section 5.1). They are based on the cyclotron motion of free carriers in both the real and the $\boldsymbol{k}$-space. Since in a QW subjected to an in-plane magnetic field the cyclotron motion is suppressed, one needs to seek alternative mechanisms. As we will demonstrate below (sections 5.3–5.5), the generation of magneto-induced photocurrent in quantum wells requires both gyrotropy and magnetic field and therefore the effects belong to the magneto-gyrotropic class.

5.1. Bulk semiconductors of the T_d point symmetry

In this section we outline briefly microscopic mechanisms responsible for magneto-photocurrents generated in bulk materials of the T_d symmetry.

Non-gyrotropic, spin-independent mechanisms. The phenomenological description of the MPGE in the T_d-class bulk crystals is given by equations (29)–(31) in appendix A.

Microscopically, the contribution proportional to S_2 in equation (29) can be easily interpreted [28, 29] as the Hall rotation of the zero-magnetic-field photocurrent. At zero magnetic field the current $\boldsymbol{j}^{(0)}$ in response to linear polarized radiation is given by

$$j_x^{(0)} \propto e_y e_z^* + e_z e_y^*, \qquad j_y^{(0)} \propto e_z e_x^* + e_x e_z^*, \qquad j_z^{(0)} \propto e_x e_y^* + e_x e_y^*.$$

Applying a magnetic field $\boldsymbol{B}$ yields a current $\boldsymbol{j}$ in the direction parallel to the vector $\boldsymbol{B} \times \boldsymbol{j}^{(0)}$. The coefficient S_1, on the other hand, determines the contribution to the photocurrent arising even if $\boldsymbol{j}^{(0)} = 0$, e.g., for $\boldsymbol{e} \parallel x$. This particular contribution can be described microscopically as follows [30] (see also [31, 32]): (a) optical alignment of free-carrier momenta described by an anisotropic correction to the free-carrier non-equilibrium distribution function, $\delta f(\boldsymbol{k})$, proportional to $k_\alpha k_\beta / k^2$; (b) new terms $k_\gamma k_\delta / k^2$ appear due to cyclotron rotation of the free-carrier distribution function; (c) momentum scattering of free carriers results in an electric current $j_\eta \propto C_{\eta+1,\eta+2}$, where $\eta = (1, 2, 3) \equiv (x, y, z)$ and $C_{\gamma,\delta}$ are the coefficients in the expansion of $\delta f(\boldsymbol{k})$ over $k_\gamma k_\delta / k^2$. Here, the cyclic permutation of indices is assumed. The current appears under one-phonon induced free carrier shifts in real space (the so-called shift contribution) or due to two-phonon asymmetric scattering (the ballistic contribution) [33, 34]. For the polarization $\boldsymbol{e} \parallel x$, the anisotropic part of the free-carrier non-equilibrium distribution function is proportional to k_x^2/k^2. For $\boldsymbol{B} \parallel y$, the cyclotron rotation of this anisotropic distribution leads to the term $\delta f(\boldsymbol{k}) \propto k_x k_z / k^2$. The further momentum relaxation yields an electric current in the y direction. It should be mentioned that a similar mechanism contributes to S_2. It is clear that both this mechanism and the photo-Hall mechanism are spin independent since the free-carrier spin is not involved here. Note that both mechanisms do exist in bulk crystals of T_d symmetry, which are non-gyrotropic. Therefore they can be classified as *non-gyrotropic* and *spin independent*.

An important point to stress is that the above mechanisms vanish in QWs for an in-plane magnetic field. Because the free-carrier motion is quantized in the growth direction the anisotropic correction $\delta f(\boldsymbol{k}) \propto k_\eta k_z / k^2$ ($\eta = x, y$) to the distribution function does not exist.

Non-gyrotropic, spin-dependent mechanisms. Two non-gyrotropic but spin-dependent mechanisms causing magnetic-field-induced photocurrents were proposed for bulk zinc-blende-lattice semiconductors in [19, 35]. In [35] the photocurrent is calculated for optical transitions between spin-split Landau-level subbands under electron spin resonance conditions in the limit of strong magnetic field. Taking into account both the spin-dependent Dresselhaus term, cubic in the wavevector $\boldsymbol{k}$,

$$\mathcal{H}^{(3)}(\boldsymbol{k}) = \gamma[\sigma_x k_x (k_y^2 - k_z^2) + \sigma_y k_y (k_z^2 - k_x^2) + \sigma_z k_z (k_x^2 - k_y^2)] \tag{8}$$

and the Zeeman term quadratic in $\boldsymbol{k}$

$$\mathcal{H}^{(2)}(\boldsymbol{B}) = \mathcal{G}(\boldsymbol{\sigma} \cdot \boldsymbol{k})(\boldsymbol{B} \cdot \boldsymbol{k}) \tag{9}$$

in the bulk electron Hamiltonian, spin-flip optical transitions lead to asymmetric photoexcitation of electrons in the $\boldsymbol{k}$-space and, hence, to a photocurrent. At a fixed radiation frequency the photocurrent has a resonant nonlinear dependence on the magnetic field and contains contributions both even and odd as a function of $\boldsymbol{B}$. In [19] the photocurrent under impurity-to-band optical transitions in bulk InSb was described taking into account the quantum interference of different transition channels, one of which includes an intermediate intra-impurity spin-flip process. This photocurrent is proportional to photon momentum and depends on the light propagation direction. Therefore, it can be classified as the photon drag effect which occurs under impurity-to-band optical transitions and is substantially modified by the intra-impurity electron spin resonance. Since in the present work the experiments were performed under normal incidence of radiation of a two-dimensional structure we will not consider the photon drag effect in the following discussion.

5.2. *Effects of gyrotropy in (001)-grown quantum wells*

The (001)-grown quantum well structures are characterized by a reduced symmetry D_{2d} (symmetric QWs) or C_{2v} (asymmetric QWs). Generally, for symmetry operations of these point groups, the in-plane components of a polar vector $\boldsymbol{R}$ and an axial vector $\boldsymbol{L}$ transform according to the same representations. In the C_{2v} group there are two invariants which can be constructed from the products $R_\alpha L_\beta$, namely,

$$\mathcal{I}_1 = R_x L_x - R_y L_y = R_{x'} L_{y'} + R_{y'} L_{x'}, \tag{10}$$

$$\mathcal{I}_2 = R_x L_y - R_y L_x = R_{x'} L_{y'} - R_{y'} L_{x'} \equiv (\boldsymbol{R} \times \boldsymbol{L})_z. \tag{11}$$

The D_{2d} symmetry allows only one invariant, $\mathcal{I}_1$. In the following $\mathcal{I}_1$- and $\mathcal{I}_2$-like functions or operators are referred to as the gyrotropic invariants.

In order to verify that a given function, $\mathcal{I}(\boldsymbol{k}', \boldsymbol{k})$, linear in $\boldsymbol{B}$ or $\boldsymbol{\sigma}$ contains a gyrotropic invariant one can use a simple criterion, namely, multiply $\mathcal{I}$ by k_η and k'_η ($\eta = x, y$), average the product over the directions of $\boldsymbol{k}'$ and $\boldsymbol{k}$ and check that the average is non-zero. Three examples of gyrotropic invariants relevant to the present work are given below.

The first is the spin–orbit part of the electron effective Hamiltonian,

$$\begin{aligned} \mathcal{H}^{(1)}_{\rm BIA} &= \beta_{\rm BIA}(\sigma_x k_x - \sigma_y k_y), & \mathcal{H}^{(1)}_{\rm SIA} &= \beta_{\rm SIA}(\sigma_x k_y - \sigma_y k_x), \\ \mathcal{H}^{(3)}_{\rm BIA} &= \gamma_{\rm BIA}(\sigma_x k_x k_y^2 - \sigma_y k_y k_x^2), & \mathcal{H}^{(3)}_{\rm SIA} &= \gamma_{\rm SIA}(\sigma_x k_y - \sigma_y k_x)k^2. \end{aligned} \tag{12}$$

Here σ_α are the spin Pauli matrices, k_x and k_y are the components of the 2D electron wavevector, $\gamma_{\rm BIA}$ coincides with the parameter γ introduced by equation (8) and $\mathcal{H}^{(1)}_{\rm BIA}$ and $\mathcal{H}^{(1)}_{\rm SIA}$ are the so-called Dresselhaus and Rashba terms, being linear in $\boldsymbol{k}$, or, respectively, bulk inversion asymmetry (BIA) and structure inversion asymmetry (SIA) terms. The terms $\mathcal{H}^{(1)}_{\rm BIA}$ and $\mathcal{H}^{(3)}_{\rm BIA}$, linear and cubic in $\boldsymbol{k}$, stem from averaging the cubic-$\boldsymbol{k}$ spin-dependent Hamiltonian equation (8).

The second example of a gyrotropic invariant is the well known diamagnetic band shift existing in asymmetric QWs [36–38]; see also [39–41]. This spin-independent contribution to the electron effective Hamiltonian reads

$$\mathcal{H}^{\rm dia}_{\rm SIA} = \tilde{\alpha}_{\rm SIA}(B_x k_y - B_y k_x). \tag{13}$$

The coefficient $\tilde{\alpha}_{\rm SIA}$ in the νth electron subband is given by $\tilde{\alpha}^{(\nu)}_{\rm SIA} = (e\hbar/cm^*)\bar{z}_\nu$, where m^* is the effective electron mass, and $\bar{z}_\nu = \langle e\nu|z|e\nu\rangle$ is the centre of mass of the electron envelope function in this subband.

The last example is an asymmetric part of electron–phonon interaction. In contrast to the previous two examples it does not modify the single-electron spectrum but can give rise to spin-dependent effects. It leads, e.g., to spin photocurrents considered in sections 5.3 and 5.4. The asymmetric part of the electron–phonon interaction is given by

$$\hat{V}_{\rm el-phon}(\boldsymbol{k}', \boldsymbol{k}) = \Xi_c \sum_j \epsilon_{jj} + \Xi_{cv}\xi \sum_j [(\boldsymbol{k}' + \boldsymbol{k}) \times \boldsymbol{\sigma}]_j \epsilon_{j+1\, j+2}. \tag{14}$$

Here $\epsilon_{jj'}$ is the phonon-induced strain tensor dependent on the phonon wavevector $\boldsymbol{q} = \boldsymbol{k}' - \boldsymbol{k}$; Ξ_c and Ξ_{cv} are the intra- and interband constants of the deformation potential. For zinc-blende-lattice QWs the coefficient ξ is given by [42]

$$\xi = \frac{i\hbar p_{cv}}{3m_0} \frac{\Delta_{\rm so}}{\varepsilon_{\rm g}(\varepsilon_{\rm g} + \Delta_{\rm so})}, \tag{15}$$

where m_0 is the free-electron mass, ε_g and Δ_{so} are the band gap and the valence band spin–orbit splitting of the bulk semiconductor used in the QW layer and $p_{cv} = \langle S|\hat{p}_z|Z\rangle$ is the interband matrix element of the momentum operator between the Bloch functions of the conduction and valence bands, S and Z.

Compared with the non-gyrotropic class T_d the presence of gyrotropic invariants in the electron effective Hamiltonian in QWs of the D_{2d} and C_{2v} symmetry enables new mechanisms of the MPGE. At present we are unaware of any non-gyrotropic mechanism of the MPGE in QW structures in the presence of an in-plane magnetic field. Thus, it is natural to classify such contributions to the MPGE as *magneto-gyrotropic photocurrents*. Below we consider microscopic mechanisms of magneto-gyrotropic photocurrents, both *spin dependent* and *spin independent*. To illustrate them we present model pictures for three different mechanisms connected to acoustic-phonon-assisted optical transitions. Optical-phonon- or defect-assisted transitions and those involving electron–electron collisions may be considered in the same way.

5.3. Photocurrent due to spin-dependent asymmetry of optical excitation

The first possible mechanism of current generation in QWs in the presence of a magnetic field is related to the asymmetry of optical excitation. The characteristic feature of this mechanism is a sensitivity to the polarization of light. In our experiments we employ free-electron absorption. Indirect optical transitions require a momentum transfer from phonons to electrons. A photocurrent induced by these transitions appears due to an asymmetry of either electron–pho*t*on or electron–pho*n*on interaction in the $\boldsymbol{k}$-space. Below we take into account the gyrotropic invariants within the first order of the perturbation theory. Therefore, while considering the spin-dependent magneto-gyrotropic effects, we can replace the contribution to the electron Hamiltonian linear in the Pauli spin matrices by only one of the terms proportional to the matrix σ_j and perform the separate calculations for each index j. Then spin-conserving and spin-flip mechanisms can be treated independently.

5.3.1. Spin-dependent spin-conserving asymmetry of photoexcitation due to asymmetric electron–phonon interaction. In gyrotropic media the electron–phonon interaction $\hat{V}_{\mathrm{el-phon}}$ contains, in addition to the main contribution, an asymmetric spin-dependent term $\propto \sigma_\alpha(k_\beta + k'_\beta)$ given by equation (14); see also [14, 42–44]. Microscopically this contribution is caused by structural and bulk inversion asymmetry like Rashba/Dresselhaus band spin splitting in the $\boldsymbol{k}$-space. The asymmetry of electron–phonon interaction results in non-equal rates of indirect optical transitions for opposite wavevectors in each spin subband with $s_\alpha = \pm 1/2$. This causes an asymmetric distribution of photoexcited carriers within the subband s_α and therefore yields a flow, $\boldsymbol{i}_\alpha$, of electrons in this subband. This situation is sketched in figure 11 for the spin-up ($s = 1/2$) subband. The single and double horizontal arrows in figure 11 indicate the difference in electron–phonon interaction strength for positive and negative wavevectors. The important point now is that single and double arrows are interchanged for the other spin direction (see equation (14)). Indeed, the enhancement of the electron–phonon interaction rate for a specific k-vector depends on the spin direction. Therefore, for the other spin subband, the situation is reversed. This is analogous to the well known spin–orbit interaction where the shift of the $\varepsilon(\boldsymbol{k})$ dispersion depends also on the spin direction. Thus without magnetic field two oppositely directed and equal currents in spin-up and spin-down subbands cancel each other exactly. This non-equilibrium electron distribution in the $\boldsymbol{k}$-space is characterized by zero electric current but non-zero pure spin current $\boldsymbol{i}_{\mathrm{spin}} = (1/2)(\boldsymbol{i}_{1/2} - \boldsymbol{i}_{-1/2})$ [45]. The application of a magnetic field results, due to the Zeeman effect, in different equilibrium populations of the subbands. This is

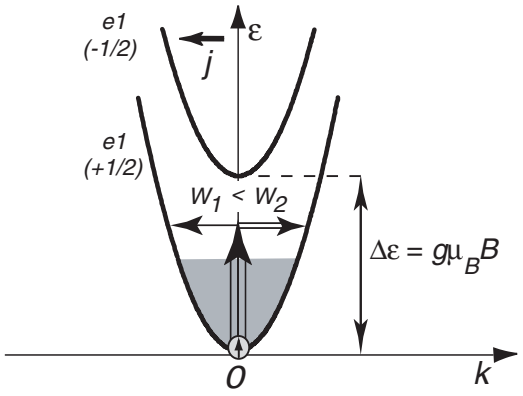

Figure 11. Microscopic origin of photocurrent caused by asymmetric photoexcitation in an in-plane magnetic field. The spin subband (+1/2) is preferentially occupied due to the Zeeman splitting. The rates of optical transitions for opposite wavevectors k are different, $W_1 < W_2$. The $\boldsymbol{k}$-linear spin splitting is neglected in the band structure because it is unimportant for this mechanism.

seen in figure 11, where the Zeeman splitting is largely exaggerated to simplify visualization. Currents flowing in opposite directions become non-equivalent, resulting in a spin-polarized net electric current. Since the current is caused by asymmetry of photoexcitation, it may depend on the polarization of radiation.

Generally, indirect optical transitions are treated in perturbation theory as second-order processes involving virtual intermediate states. The compound matrix element of phonon-mediated transition $(s, \boldsymbol{k}) \to (s', \boldsymbol{k}')$ with the intermediate state in the same subband e1 can be written as

$$M^{(\pm)}_{s'\boldsymbol{k}',s\boldsymbol{k}} = \sum_{s''} \left[\frac{V^{(\pm)}_{s'\boldsymbol{k}',s''\boldsymbol{k}} R_{s'',s}(\boldsymbol{k})}{\varepsilon_s(\boldsymbol{k}) - \varepsilon_{s''}(\boldsymbol{k}) + \hbar\omega} + \frac{R_{s',s''}(\boldsymbol{k}') V^{(\pm)}_{s''\boldsymbol{k}',s\boldsymbol{k}}}{\varepsilon_s(\boldsymbol{k}) - \varepsilon_{s''}(\boldsymbol{k}') \mp \hbar\Omega(\boldsymbol{q})} \right], \tag{16}$$

where $R_{s',s}(\boldsymbol{k})$ is the direct optical matrix element, $V^{(\pm)}_{s'\boldsymbol{k}',s\boldsymbol{k}}$ is the matrix element of phonon-induced scattering, the upper (lower) sign in $\pm$ and $\mp$ means the indirect transition involving absorption (emission) of a phonon and s, s' and s'' are the spin indices.

While considering the spin-conserving electron transitions, we use the basis of electron states with the spin components $s = \pm 1/2$ parallel to the direction $\eta \parallel \boldsymbol{B}$, retain in the gyrotropic invariants only the spin-independent terms containing σ_η and consider the processes $(s, \boldsymbol{k}) \to (s, \boldsymbol{k}')$. Then, in equation (16) one can set $s = s' = s''$ and reduce the equation to

$$M^{(\pm)}_{s\boldsymbol{k}',s\boldsymbol{k}} = V^{(\pm)}_{s\boldsymbol{k}',s\boldsymbol{k}} [R_{s,s}(\boldsymbol{k}) - R_{s,s}(\boldsymbol{k}')]/\hbar\omega. \tag{17}$$

The photocurrent density is given by

$$\boldsymbol{j} = e\frac{2\pi}{\hbar} \sum_{\boldsymbol{k}'\boldsymbol{k}s\pm} [\boldsymbol{v}_s(\boldsymbol{k}')\tau'_p - \boldsymbol{v}_s(\boldsymbol{k})\tau_p] |M^{(\pm)}_{s\boldsymbol{k}',s\boldsymbol{k}}|^2 \{ f^0_s(\boldsymbol{k})[1 - f^0_s(\boldsymbol{k}')] N^{(\pm)}_{\boldsymbol{q}} - f^0_s(\boldsymbol{k}')[1 - f^0_s(\boldsymbol{k})] N^{(\mp)}_{\boldsymbol{q}} \} \delta[\varepsilon_s(\boldsymbol{k}') - \varepsilon_s(\boldsymbol{k}) - \hbar\omega \pm \hbar\Omega(\boldsymbol{q})], \tag{18}$$

where e is the electron charge, $\boldsymbol{v}_s(\boldsymbol{k})$ is the electron group velocity in the state $(s, \boldsymbol{k})$, τ_p and τ'_p are the electron momentum relaxation times in the initial and final states, $f^0_s(\boldsymbol{k})$ is the electron equilibrium distribution function, $\boldsymbol{q} = \boldsymbol{k}' - \boldsymbol{k}$ is the phonon wavevector, $N^{(\pm)}_{\boldsymbol{q}} = N_{\boldsymbol{q}} + (1 \pm 1)/2$ and $N_{\boldsymbol{q}}$ is the phonon occupation number.

For the mechanism in question one retains in $R_{s,s}(\boldsymbol{k})$ the main contribution $-(eA_0/cm^*)(\hbar\boldsymbol{k} \cdot \boldsymbol{e})$ and uses the electron–phonon interaction in the form of equation (14), which can be rewritten as

$$V_{s\boldsymbol{k}',s\boldsymbol{k}} = \Xi_c \epsilon_{ii} + \Xi_{cv} \xi [(\boldsymbol{k}' + \boldsymbol{k}) \times \boldsymbol{\sigma}_{ss}]_z \, \epsilon_{xy}. \tag{19}$$

Here A_0, $\boldsymbol{e}$ are the scalar amplitude and polarization unit vector of the light vector potential, and $\epsilon_{ii} \equiv \sum_i \epsilon_{ii}$.

Under indirect photoexcitation, the asymmetry of scattering described by equation (19) leads to electric currents of opposite directions in both spin subbands. The net electric current occurs due to the Zeeman-splitting-induced selective occupation of these branches in equilibrium. We recall that, in the first order in the magnetic field $\boldsymbol{B}$, the average equilibrium electron spin is given by

$$\boldsymbol{S}^{(0)} = -\frac{g\mu_{\mathrm{B}}\boldsymbol{B}}{4\bar{\varepsilon}}, \tag{20}$$

where g is the electron effective g-factor, μ_{B} is the Bohr magneton, $\bar{\varepsilon}$ is the characteristic electron energy defined for the 2D gas as $\int \mathrm{d}\varepsilon\, f(\varepsilon)/f(0)$, with $f(\varepsilon)$ being the equilibrium distribution function at zero field, so that $\bar{\varepsilon}$ equals the Fermi energy, ε_{F}, and the thermal energy, $k_{\mathrm{B}}T$, for degenerate and non-degenerate electron gas, respectively. The current, induced by electron–phonon asymmetry under indirect photoexcitation, can be estimated as

$$j \propto \frac{e\tau_p}{\hbar}\frac{\Xi_{cv}\xi}{\Xi_c}\eta_{\mathrm{ph}} I S^{(0)},$$

where η_{ph} is the phonon-assisted absorbance of the terahertz radiation.

For impurity-assisted photoexcitation, instead of equation (19), one can use the spin-dependent matrix element of scattering by an impurity,

$$V_{s\boldsymbol{k}',s\boldsymbol{k}} = \{V_0(\boldsymbol{q}) + V_z(\boldsymbol{q})\,\xi[(\boldsymbol{k}'+\boldsymbol{k})\times\boldsymbol{\sigma}_{ss}]_z\}\mathrm{e}^{\mathrm{i}(\boldsymbol{k}-\boldsymbol{k}')\boldsymbol{r}_{\mathrm{im}}}, \tag{21}$$

where $\boldsymbol{q} = \boldsymbol{k}' - \boldsymbol{k}$, V_0 is the matrix element for intraband electron scattering by the defect, V_z is the matrix element of the defect potential taken between the conduction-band Bloch function S and the valence-band function Z (see [42] for details) and $\boldsymbol{r}_{\mathrm{im}}$ is the in-plane position of the impurity.

5.3.2. Asymmetry of photoexcitation due to asymmetrical electron–phonon spin-flip scattering. Indirect optical transitions involving phonon-induced asymmetric spin-flip scattering also lead to an electric current if spin subbands are selectively occupied due to Zeeman splitting. The asymmetry can be due to a dependence of the spin-flip scattering rate on the transferred wavevector $\boldsymbol{k}' - \boldsymbol{k}$ in the system with the odd-$\boldsymbol{k}$ spin splitting of the electron subbands; see [7]. Estimations show that this mechanism to the photocurrent is negligible compared to the previous mechanism 5.3.1.

5.3.3. Spin-dependent spin-conserving asymmetry of photoexcitation due to asymmetric electron–photon interaction. A magnetic-field-induced photocurrent under linearly polarized excitation can occur due to an asymmetry of electron–photon interaction. The asymmetry is described by the optical matrix element

$$R_{s,s}(\boldsymbol{k}) = -\frac{eA_0}{c}\left[\frac{\hbar(\boldsymbol{k}\cdot\boldsymbol{e})}{m^*} + \frac{1}{\hbar}\sum_j e_j\frac{\partial}{\partial k_j}\mathcal{H}^{(3)}_{ss}(\boldsymbol{k};\eta)\right], \tag{22}$$

where $\mathcal{H}^{(3)}_{ss}(\boldsymbol{k};\eta)$ is the σ_η-dependent term in the cubic-$\boldsymbol{k}$ contribution $\mathcal{H}^{(3)}_{\mathrm{BIA}}(\boldsymbol{k}) + \mathcal{H}^{(3)}_{\mathrm{SIA}}(\boldsymbol{k})$ to the electron Hamiltonian. Here, for the electron–phonon matrix element, one can take the main spin-independent contribution including both the piezoelectric and deformation-potential mechanisms. Under indirect light absorption, the electron–photon asymmetry results in electric currents flowing in opposite directions in both spin branches. Similarly to the mechanism 5.3.1, the net electric current is non-zero due to the selective occupation of the Zeeman-split spin branches.

It should be stressed that the $\mathcal{H}^{(3)}_{ss}(\boldsymbol{k};\eta)$ term should also be taken into account in the δ-function, the distribution function and the group velocity in the microscopic expression (18) for the photocurrent. Note that the linear-$\boldsymbol{k}$ terms in the effective electron Hamiltonian (see equation (12)) do not lead to a photocurrent in the first order in $\beta_{\rm BIA}$ or $\beta_{\rm SIA}$ because the linear-k_i term in the function $\hbar^2 k_i^2/2m^* + \beta k_i$ disappears after the replacement $k_i \to \tilde{k}_i = k_i + \beta m^*/\hbar^2$.

5.3.4. Asymmetry of spin-flip photoexcitation due to asymmetric electron–photon interaction. To obtain the asymmetric photoexcitation for optical spin-flip processes we can take into account, along with the term odd-$\boldsymbol{k}$, the quadratic-$\boldsymbol{k}$ Zeeman term similar to that introduced by equation (9). Then the spin-flip optical matrix element is given by

$$R_{\bar{s},s}(\boldsymbol{k}) = -\frac{eA_0}{\hbar c}\left\{\mathcal{G}\boldsymbol{\sigma}_{\bar{s},s}\cdot[e(\boldsymbol{B}\cdot\boldsymbol{k}) + \boldsymbol{k}(\boldsymbol{B}\cdot\boldsymbol{e})] + \sum_j e_j \frac{\partial}{\partial k_j}\mathcal{H}_{\bar{s},s}(\boldsymbol{k})\right\}, \quad (23)$$

where $\bar{s} = -s$ and $\mathcal{H}(\boldsymbol{k})$ is the odd-$\boldsymbol{k}$ contribution to the electron Hamiltonian, including both linear and cubic terms. Estimations show that the photocurrent due to the spin-conserving processes described by equation (22) is larger than that due to the spin-flip processes described by equation (23).

5.3.5. Spin-dependent asymmetry of indirect transitions via other bands or subbands. This contribution is described by equation (16) where the summation is performed over virtual states in subbands different from e1. The estimation shows that it is of the same order of magnitude as the contribution due to the mechanism 5.3.1.

Summarizing the above mechanisms we would like to stress that the characteristic feature of all of them is a sensitivity to the light linear polarization described in equations (3) by the terms proportional to S_2, S_2', S_3, S_3'. Depending on the particular set of parameters, e.g., those in equations (12), (14), the energy dependence of τ_p, the ratio between the photon energy, the electron average energy etc, one can obtain any value for the ratio between S_2 and S_3 as well as for the ratio between one of them and the coefficient S_1.

5.4. Current due to spin-dependent asymmetry of electron relaxation

Energy and spin relaxation of a non-equilibrium electron gas in gyrotropic systems can also drive an electric current. The current is a result of relaxation of heated carriers, and hence its magnitude and direction are independent of the polarization of radiation. Several mechanisms related to the asymmetry of electron relaxation are considered below.

5.4.1. Asymmetry of electron energy relaxation. Another mechanism which stems from spin-dependent asymmetric terms in the electron–phonon interaction is the energy relaxation of hot carriers [14]. The light absorption by free electrons leads to an electron gas heating, i.e. to a non-equilibrium energy distribution of electrons. Here we assume, for simplicity, that the photoexcitation results in isotropic non-equilibrium distribution of carriers. Due to asymmetry of electron–phonon interaction discussed above (see equation (14) and section 5), hot electrons with opposite $\boldsymbol{k}$ have different relaxation rates. This situation is sketched in figure 12 for a spin-up subband ($s = 1/2$), where two arrows of different thicknesses denote non-equal relaxation rates. As a result, an electric current is generated. Whether $-k$ or $+k$ states relax preferentially depends on the spin direction. This is because the electron–phonon asymmetry is spin dependent and has the opposite sign in the other spin subband. Similarly

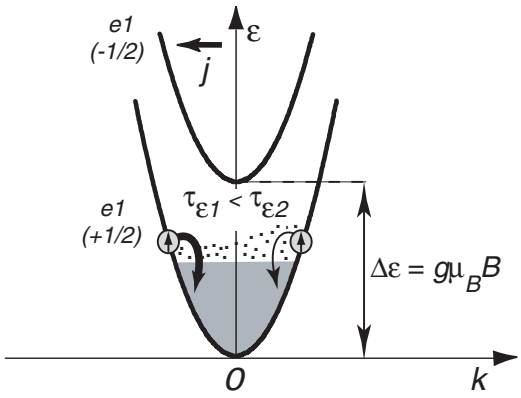

Figure 12. Microscopic origin of the electric current caused by asymmetry of the energy relaxation in the presence of an in-plane magnetic field. The spin subband (+1/2) is preferably occupied due to the Zeeman splitting. The $\boldsymbol{k}$-linear spin splitting is neglected in the band structure because it is unimportant for this mechanism.

to the case described in mechanism 5.3.1, the arrows in figure 12 need to be interchanged for the other spin subband. For $B = 0$ the currents in the spin-up and spin-down subbands have opposite directions and cancel exactly. But as described in section 5.3.1 a pure spin current flows which accumulates opposite spins at opposite edges of the sample. In the presence of a magnetic field the currents moving in the opposite directions do not cancel due to the non-equal population of the spin subbands (see figure 12) and a net electric current flows.

For the electron–phonon interaction given by equation (14) one has

$$V_{s_x\boldsymbol{k}',s_x\boldsymbol{k}} = \Xi_c\varepsilon_{ii} - \Xi_{cv}\xi(k'_y + k_y)\epsilon_{xy}\,\mathrm{sgn}\,s_x. \tag{24}$$

Thus, the ratio of antisymmetric to symmetric parts of the scattering probability rate, $W_{s_x\boldsymbol{k}',s_x\boldsymbol{k}} \propto |V_{s_x\boldsymbol{k}',s_x\boldsymbol{k}}|^2$, is given by $W_{\mathrm{as}}/W_{\mathrm{s}} \sim (\Xi_{cv}\xi\epsilon_{xy}/\Xi_c\epsilon_{ii})(k'_y + k_y)$. Since the antisymmetric component of the electron distribution function decays within the momentum relaxation time τ_p, one can write for the photocurrent

$$j_i \sim eN\frac{g\mu_{\mathrm{B}}B_x}{\bar{\varepsilon}}\left\langle W_{\mathrm{s}}\frac{\Xi_{cv}\xi}{\Xi_c}\frac{\epsilon_{xy}(k'_y + k_y)}{\epsilon_{ii}}\left[\tau_p(k')\frac{\hbar k'_i}{m^*} - \tau_p(k)\frac{\hbar k_i}{m^*}\right]\right\rangle,$$

where N is the 2D electron density and the angle brackets mean averaging over the electron energy distribution. While the average for j_y is zero, the x component of the photocurrent can be estimated as

$$j_x \sim \frac{e\tau_p}{\hbar}\frac{\Xi_{cv}\xi}{\Xi_c}\frac{g\mu_{\mathrm{B}}B_x}{\bar{\varepsilon}}\eta I, \tag{25}$$

where η is the fraction of the energy flux absorbed in the QW due to all possible indirect optical transitions. By deriving this equation we took into account the balance of energy

$$\sum_{\boldsymbol{k}'\boldsymbol{k}}[\varepsilon(\boldsymbol{k}) - \varepsilon(\boldsymbol{k}')]W_{\boldsymbol{k}',\boldsymbol{k}} = \eta I,$$

where $\varepsilon(\boldsymbol{k}) = \hbar^2k^2/2m^*$. An additional contribution to the relaxation photocurrent comes if we neglect the asymmetry of electron–phonon interaction by setting $\xi = 0$ but, instead, take cubic-$\boldsymbol{k}$ terms into account in the electron effective Hamiltonian.

Compared to the mechanisms 5.3, the main characteristic feature of mechanism 5.4.1 is its independence of the in-plane linear-polarization orientation, i.e. $S_2 = S'_2 = S_3 = S'_3 = 0$. A particular choice of $V_{s_x\boldsymbol{k}',s_x\boldsymbol{k}}$ in the form of equation (24) leads to a photocurrent with $S'_1 = S_1$ or, equivalently, $S_1^- = 0$. By adding a spin-dependent invariant of the type $\mathcal{I}_2$ to the right-hand part of equation (24) one can also obtain a non-zero value of S_1^-.

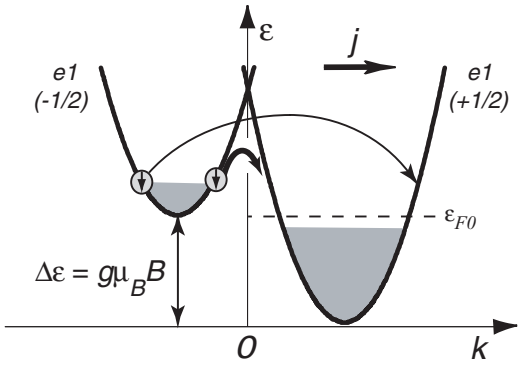

Figure 13. Microscopic origin of the electric current caused by asymmetry of spin relaxation. Non-equilibrium spin is due to photoinduced depolarization of electron spins. Asymmetry of spin relaxation and, hence, an electric current is caused by $\boldsymbol{k}$-linear spin splitting.

5.4.2. Current due to spin-dependent asymmetry of spin relaxation (spin-galvanic effect). This mechanism is based on the asymmetry of spin-flip relaxation processes and represents in fact the spin-galvanic effect [7] where the current is linked to spin polarization

$$j_i = Q_{ii'}(S_{i'} - S_{i'}^{(0)}). \tag{26}$$

Here $\boldsymbol{S}$ is the average electron spin and $\boldsymbol{S}^{(0)}$ is its equilibrium value; see equation (20). In contrast to the majority of the mechanisms considered above which do not contain $\boldsymbol{k}$-linear terms, these are crucial here.

In the previous considerations the spin-galvanic effect was described for a non-equilibrium spin polarization achieved by optical orientation where $\boldsymbol{S}^{(0)}$ was negligible [3, 7]. Here we discuss a more general situation: a non-zero $\boldsymbol{S}^{(0)}$ caused by the Zeeman splitting in a magnetic field is explicitly taken into account. We show below that in addition to optical orientation with circularly polarized light, it opens a new possibility to achieve a non-equilibrium spin polarization and, hence, an additional contribution to the photocurrent.

Figure 13 illustrates this mechanism. In equilibrium the electrons preferably occupy the Zeeman split lower spin subband. By optical excitation with light of any polarization a non-equilibrium population as sketched in figure 13 can be achieved. This is a consequence of the fact that optical transitions from the highly occupied subband dominate. These optically excited electrons under energy relaxation return to both subbands. Thus, a non-equilibrium population of the spin subbands appears. To return to equilibrium, spin-flip transitions are required. Since spin relaxation efficiently depends on initial and final k-vectors, the presence of k-linear terms leads to an asymmetry of spin relaxation (see bent arrows in figure 13), and hence to current flow. This mechanism was described in [7].

Following similar arguments as in [7, 46] one can estimate the spin-galvanic contribution to the polarization-independent magneto-induced photocurrent as

$$j \sim e\tau_p \frac{\beta}{\hbar} \frac{g\mu_B B}{\bar{\varepsilon}} \frac{\eta I}{\hbar\omega} \zeta. \tag{27}$$

Here ζ is a factor describing the electron spin depolarization due to photoexcitation followed by the energy relaxation. It can be estimated as $\zeta \sim \tau_\varepsilon/\tau_s$, where τ_ε is the electron energy relaxation time governed mainly by electron–electron collisions, and τ_s is the spin relaxation time. Assuming $\tau_\varepsilon \sim 10^{-13}$ s and $\tau_s \sim 10^{-10}$ s at room temperature, the factor ζ is estimated as 10^{-3}.

5.5. Spin-independent mechanisms of magneto-induced photocurrent

The last group of mechanisms is based on a magnetic-field-induced shift of the energy dispersion in the $\boldsymbol{k}$-space in gyrotropic materials. This mechanism was investigated theoretically and observed experimentally for direct interband transitions [21, 22] and proved to be efficient. To obtain such a current for indirect optical transitions one should take into account effects of the second order like non-parabolicity or transitions via virtual states in the other bands. Our estimations show that these processes are less efficient compared to mechanisms 5.3 and 5.4. However, to be complete, we consider below possible contributions of the diamagnetic shift to the current at the Drude absorption of radiation.

5.5.1. Spin-independent asymmetry of indirect transitions with intermediate states in the same subband. The experiments on the MPGE under direct optical transitions observed in asymmetric QW structures are interpreted in terms of the asymmetric spin-independent electron energy dispersion, $\varepsilon(\boldsymbol{k}, \boldsymbol{B}) \neq \varepsilon(-\boldsymbol{k}, \boldsymbol{B})$, analysed by Gorbatsevich *et al* [16]; see also [17, 18]. The simplest contribution to the electron effective Hamiltonian representing such a kind of asymmetric dispersion is the diamagnetic term $\mathcal{H}_{\rm SIA}^{\rm (dia)}$ in equation (13). In asymmetric QWs, $\bar{z}_\nu$ are non-zero and the subband dispersion is given by parabolas with their minima (or maxima in case of the valence band) shifted from the origin $k_x = k_y = 0$ by a value proportional to the in-plane magnetic field.

For indirect optical transitions these linear-$\boldsymbol{k}$ terms do not lead, in the first order, to a photocurrent. To obtain the current one needs to take into account the non-parabolic diamagnetic term

$$\mathcal{H}_{\rm SIA}^{\rm (dia,3)} = \mathcal{F}_{\rm SIA}(B_x k_y - B_y k_x)k^2. \tag{28}$$

The non-parabolicity parameter can be estimated by $\mathcal{F}_{\rm SIA} \sim (\hbar^2/m^* E_{\rm g})\tilde{\alpha}_{\rm SIA}$. By analogy with the SIA diamagnetic term we can introduce the BIA diamagnetic term $\mathcal{H}_{\rm BIA}^{\rm (dia,3)} = \mathcal{F}_{\rm BIA}(B_x k_x - B_y k_y)k^2$. It is most likely that, in realistic QWs, the coefficient $\mathcal{F}_{\rm BIA}$ is small as compared to $\mathcal{F}_{\rm SIA}$.

5.5.2. Spin-independent asymmetry of indirect transitions via other bands and subbands. One can show that even the linear-$\boldsymbol{k}$ diamagnetic terms can contribute to the photocurrent under indirect intra-subband optical transitions if the indirect transition involves intermediate states in other bands (or subbands) different from the conduction subband e1. Under normal incidence of the light, a reasonable choice could be a combination of direct intraband optical transitions with the piezoelectric electron–phonon interaction for the first process, and interband virtual optical transitions as well as interband deformation-potential electron–phonon interaction for the second process. An asymmetry of the indirect photoexcitation is obtained as a result of the interference between two indirect processes with the intermediate state in the same subband and elsewhere. Moreover, the diamagnetic dispersion asymmetry of the initial and intermediate bands should be taken into account in the energy denominator of the compound two-quantum matrix element for the transitions via other bands.

5.5.3. Spin-independent asymmetry of electron energy relaxation. Similarly to the spin-dependent mechanism 5.4.1, the diamagnetic cubic-$\boldsymbol{k}$ term (see equation (28)) can be responsible for the relaxational photocurrent. This relaxation mechanism is unlikely to give an essential contribution to the MPGE.

To summarize this group of mechanisms we note that, as in the case of spin-dependent mechanisms, mechanisms 5.5.1 and 5.5.2 allow a pronounced dependence of the photocurrent

on the orientation of the in-plane light polarization whereas the relaxation mechanism 5.5.3 is independent of the polarization state.

6. Discussion

In all investigated QW structures, illumination with terahertz radiation in the presence of an in-plane magnetic field results in a photocurrent in full agreement with the phenomenological theory described by equations (3). The microscopic treatment presented in section 5 shows that two classes of mechanisms dominate the magneto-gyrotropic effects. The current may be induced either by an asymmetry of optical excitation and/or by an asymmetry of relaxation. Though in all cases the absorption is mainly independent of the light polarization, the photocurrent depends on polarization for the first class of the mechanisms (see section 5.3) but is independent of the direction of linear light polarization for the second class (see section 5.4). Thus the polarization dependence of the magneto-gyrotropic photocurrent signals allows us to distinguish between the above two classes. The asymmetry of photoexcitation may contribute to all terms in equations (3). Therefore, such photocurrent contributions should exhibit a characteristic polarization dependence given, for linearly polarized light, by the second and third terms in equations (3) with the coefficients S_2, S_2', S_3 and S_3'. In contrast, the asymmetry of relaxation processes (see section 5.4) contributes only to the coefficients S_1, S_1', S_4 and S_4'.

The experimental data obtained on samples A1–A4 suggest that in these QW structures relaxation mechanisms, presented in section 5.4, dominate. Indeed only current contributions described by the first and last terms in equations (3) are detectable, whereas the second- and third-term contributions are vanishingly small. These samples are denoted as type I below. The results obtained for type I samples are valid in the wide temperature range from 4.2 K up to room temperature. The transverse photocurrent observed in the direction normal to the magnetic field $\boldsymbol{B}$ applied along $\langle 110 \rangle$ is independent of the light polarization. It corresponds to the first term in equations (3). Hence, this current is caused by the Drude absorption-induced electron gas heating followed by energy relaxation (mechanism 5.4.1) and/or spin relaxation (mechanism 5.4.2). The analysis (see section 5.4) shows that in the absence of the magnetic field electron gas heating in gyrotropic QWs is accompanied by a pure spin flow. The longitudinal photocurrent component parallel to $\boldsymbol{B}$, which appears under excitation with circularly polarized radiation only, arises due to spin relaxation of optically oriented carriers (spin-galvanic effect [3, 7]).

In contrast to the samples of type I, the experimental results obtained on sample A5 (in the following denoted as type II) has characteristic polarization dependences corresponding to the second (S_2, S_2') and third (S_3, S_3') terms in equations (3). The photocurrent exhibits a pronounced dependence on the azimuthal angle α of the linear polarization, but it is equal for the right and left circular polarized light. This experimental finding proves that the main mechanism for current generation in a type II sample is the asymmetry of photoexcitation considered in section 5.3.

The question concerning the difference of type I and type II samples remains open. While experimentally the two classes of mechanisms are clearly observed, it is not clear yet what determines the large difference between the relevant S-coefficients. Not much difference is expected between the type I and II samples regarding the strength and asymmetry of electron–phonon interaction. The samples only differ in the type of doping and the electron mobility. The influence of impurity potentials (density, position, scattering mechanisms etc) on a microscopic level still needs to be explored. In addition, the doping level of the type I samples is significantly lower and the mobility is higher than those in the type II samples. This can also affect the interplay between the excitation and relaxation mechanisms.

Finally we note that under steady-state optical excitation the contributions of the relaxation and photoexcitation mechanisms to magneto-induced photogalvanic effects are superimposed. However, they can be separated experimentally in time-resolved measurements. Indeed, under ultra-short pulsed photoexcitation the current should decay, for the mechanisms considered above, within the energy (τ_ε), spin (τ_s) and momentum (τ_p) relaxation times.

7. Summary

We have studied photocurrents in n-doped zinc-blende-based (001)-grown QWs generated by the Drude absorption of normally incident terahertz radiation in the presence of an in-plane magnetic field. The results agree with the phenomenological description based on the symmetry. Both experiment and theoretical analysis show that there are a variety of routes to generate spin-polarized currents. As we used both magnetic fields and gyrotropic mechanisms we coined the notation 'magneto-gyrotropic photogalvanic effects' for this class of phenomena.

Acknowledgments

The high-quality InAs quantum wells were kindly provided by J De Boeck and G Borghs from IMEC Belgium. We thank L E Golub for helpful discussion. This work was supported by the DFG, the RFBR, the INTAS, programmes of the RAS and Foundation 'Dynasty'—ICFPM.

Appendix A. Point groups T_d and D_{2d}

In the T_d-class bulk crystals the MPGE linear in the magnetic field $\boldsymbol{B}$ can be phenomenologically presented as [28, 47]

$$\begin{aligned} j_x = {} & 2S_1(|e_y|^2 - |e_z|^2)B_x I + S_2[(e_z e_x^* + e_x e_z^*)B_z - (e_x e_y^* + e_y e_x^*)B_y]I \\ & - S_4[\mathrm{i}(\boldsymbol{e}\times\boldsymbol{e}^*)_y B_z + \mathrm{i}(\boldsymbol{e}\times\boldsymbol{e}^*)_z B_y]I, \end{aligned} \tag{29}$$

and similar expressions for j_y and j_z, where $x \parallel [100]$, $y \parallel [010]$ and $z \parallel [001]$. Note that here the notation of the coefficients is chosen as to be in accordance with the phenomenological equations (7). Under photoexcitation along the [001] axis, $e_z = 0$ and, in the presence of an external magnetic field $\boldsymbol{B} \perp [001]$, one has

$$\begin{aligned} j_x &= S_1[1 - (|e_x|^2 - |e_y|^2)]B_x I - B_y I\left[S_2\left(e_x e_y^* + e_y e_x^*\right) + S_4 P_{\mathrm{circ}}\right], \\ j_y &= -S_1[1 + (|e_x|^2 - |e_y|^2)]B_y I + B_x I\left[S_2\left(e_x e_y^* + e_y e_x^*\right) - S_4 P_{\mathrm{circ}}\right]. \end{aligned} \tag{30}$$

In the axes $x' \parallel [1\bar{1}0]$, $y' \parallel [110]$, $z \parallel [001]$, equations (30) assume the form

$$\begin{aligned} j_{x'} &= S_1\left[B_{y'} - \left(e_{x'}e_{y'}^* + e_{y'}e_{x'}^*\right)B_{x'}\right]I + S_2\left(|e_{x'}|^2 - |e_{y'}|^2\right)B_{y'}I + S_4 P_{\mathrm{circ}} B_{x'} I, \\ j_{y'} &= S_1\left[B_{x'} - \left(e_{x'}e_{y'}^* + e_{y'}e_{x'}^*\right)B_{y'}\right]I - S_2\left(|e_{x'}|^2 - |e_{y'}|^2\right)B_{x'}I - S_4 P_{\mathrm{circ}} B_{y'} I. \end{aligned} \tag{31}$$

Equations (30), (31) are consistent with equations (3), (7) describing the magneto-induced photocurrents in the C_{2v}-symmetry systems and can be obtained from equations (3), (7) by setting $S_1' = S_1 = -S_3 = -S_3'$, $S_2' = -S_2$ or, equivalently, $S_1^- = S_2^+ = S_3^- = S_4^+ = 0$ and $S_1^+ = -S_3^+ = S_1$, $S_2^- = S_2$, $S_4^- = S_4$.

One can show that the phenomenological equations for the D_{2d} symmetry are obtained from equations (3), (7) if we set $S_1' = S_1$, $S_3 = S_3'$, $S_2' = -S_2$ and $S_4' = -S_4$. The only difference from equations (30), (31) is that S_1 and S_3 are now linearly independent.

Appendix B. Point group $C_{\infty v}$

For a system of the $C_{\infty v}$ symmetry, one has

$$\begin{aligned} j_x &= S_1 B_y I + S_2 \left[\left(|e_x|^2 - |e_y|^2 \right) B_y - \left(e_x e_y^* + e_y e_x^* \right) B_x \right] I + S_4 B_x I P_{\mathrm{circ}}, \\ j_y &= -S_1 B_x I + S_2 \left[\left(|e_x|^2 - |e_y|^2 \right) B_x + \left(e_x e_y^* + e_y e_x^* \right) B_y \right] I + S_4 B_y I P_{\mathrm{circ}}, \end{aligned} \tag{32}$$

where the form of the equation is independent of the orientation of Cartesian coordinates (x, y) in a plane normal to the C_∞-axis. A comparison to equations (3) for C_{2v} symmetry shows that the form of these equations is identical besides the coefficients S_i. In this case we have $S_1' = -S_1$, $S_2 = S_2' = -S_3 = S_3'$ and $S_4' = S_4$.

References

[1] Wolf S A *et al* 2001 *Science* **294** 1448
[2] Ivchenko E L 2002 *Usp. Fiz. Nauk* **45** 1461
Ivchenko E L 2002 *Phys. Usp.* **45** 1299 (Engl. Transl.)
[3] Ganichev S D and Prettl W 2003 *J. Phys.: Condens. Matter* **15** R935
[4] Averkiev N S and D'yakonov M I 1983 *Fiz. Tekh. Poluprov.* **17** 629
Averkiev N S and D'yakonov M I 1983 *Sov. Phys.—Semicond.* **17** 393 (Engl. Transl.)
[5] D'yakonov M I and Perel' V I 1971 *Pis. Zh. Eksp. Teor. Fiz.* **13** 206
D'yakonov M I and Perel' V I 1971 *JETP Lett.* **13** 144 (Engl. Transl.)
[6] Bakun A A, Zakharchenya B P, Rogachev A A, Tkachuk M N and Fleisher V G 1984 *Pis. Zh. Eksp. Teor. Fiz.* **40** 464
Bakun A A, Zakharchenya B P, Rogachev A A, Tkachuk M N and Fleisher V G 1985 *JETP Lett.* **40** 1293 (Engl. Transl.)
[7] Ganichev S D, Ivchenko E L, Bel'kov V V, Tarasenko S A, Sollinger M, Weiss D, Wegscheider W and Prettl W 2002 *Nature* **417** 153
[8] Ganichev S D, Ivchenko E L, Danilov S N, Eroms J, Wegscheider W, Weiss D and Prettl W 2001 *Phys. Rev. Lett.* **86** 4358
[9] Bhat R D R and Sipe J E 2000 *Phys. Rev. Lett.* **85** 5432
[10] Stevens M J, Smirl A L, Bhat R D R, Sipe J E and van Driel H M 2002 *J. Appl. Phys.* **91** 4382
[11] Žutić I, Fabian J and Das Sarma S 2001 *Appl. Phys. Lett.* **79** 1558
Žutić I, Fabian J and Das Sarma S 2002 *Phys. Rev. Lett.* **88** 066603
[12] Meier F and Zakharchenya B P (ed) 1984 *Optical Orientation* (Amsterdam: Elsevier Science)
[13] Ivchenko E L and Pikus G E 1978 *Pis. Zh. Eksp. Teor. Fiz.* **27** 640
Ivchenko E L and Pikus G E 1978 *JETP Lett.* **27** 604 (Engl. Transl.)
[14] Ivchenko E L and Pikus G E 1983 *Izv. Akad. Nauk SSSR Ser. Fiz.* **47** 2369
Ivchenko E L and Pikus G E 1983 *Bull. Acad. Sci. USSR Phys. Ser.* **47** 81 (Engl. Transl.)
[15] Magarill L I 1990 *Fiz. Tverd. Tela* **32** 3558
Magarill L I 1990 *Sov. Phys.—Solid State* **32** 2064 (Engl. Transl.)
[16] Gorbatsevich A A, Kapaev V V and Kopaev Yu V 1993 *Pis. Zh. Eksp. Teor. Fiz.* **57** 565
Gorbatsevich A A, Kapaev V V and Kopaev Yu V 1993 *JETP Lett.* **57** 580 (Engl. Transl.)
[17] Kibis O V 2002 *Physica* E **12** 741
[18] Ivchenko E L and Spivak B 2002 *Phys. Rev.* B **66** 155404
[19] Dmitriev A P, Emel'yanov S A, Terent'ev Ya V and Yaroshetskii I D 1989 *Pis. Zh. Eksp. Teor. Fiz.* **49** 506
Dmitriev A P, Emel'yanov S A, Terent'ev Ya V and Yaroshetskii I D 1989 *JETP Lett.* **49** 584 (Engl. Transl.)
Dmitriev A P, Emel'yanov S A, Terent'ev Ya V and Yaroshetskii I D 1989 *Solid State Commun.* **72** 1149
Dmitriev A P, Emel'yanov S A, Terent'ev Ya V and Yaroshetskii I D 1991 *Zh. Eksp. Teor. Fiz.* **99** 619
Dmitriev A P, Emel'yanov S A, Terent'ev Ya V and Yaroshetskii I D 1991 *JETP* **72** 347 (Engl. Transl.)
[20] Dmitriev A P, Emel'yanov S A, Ivanov S V, Kop'ev P S, Terent'ev Ya V and Yaroshetskii I D 1991 *Pis. Zh. Eksp. Teor. Fiz.* **54** 279
Dmitriev A P, Emel'yanov S A, Ivanov S V, Kop'ev P S, Terent'ev Ya V and Yaroshetskii I D 1991 *JETP Lett.* **54** 273 (Engl. Transl.)
[21] Aleshchenko Yu A, Voronova I D, Gri-shechkina S P, Kapaev V V, Kopaev Yu V, Kucherenko I V, Kadushkin V I and Fomichev S I 1993 *Pis. Zh. Eksp. Teor. Fiz.* **58** 377

Aleshchenko Yu A, Voronova I D, Gri-shechkina S P, Kapaev V V, Kopaev Yu V, Kucherenko I V, Kadushkin V I and Fomichev S I 1993 *JETP Lett.* **58** (Engl. Transl.)
[22] Kucherenko I V, Vodop'yanov L K and Kadushkin V I 1997 *Fiz. Tekh. Poluprov.* **31** 872
Kucherenko I V, Vodop'yanov L K and Kadushkin V I 1997 *Semiconductors* **31** 740 (Engl. Transl.)
[23] Wunderlich J, Kästner B, Sinova J and Jungwirth T 2004 *Preprint* cond-mat/0410295
[24] Kato Y K, Myers R C, Gossard A C and Awschalom D D 2004 *Science* **306** 1910
[25] Beneth M, Nemeth S, De Boeck J, Borghs G, Tümmler J, Woitok J and Geurts J 1998 *Semicond. Sci. Technol.* **13** 428
[26] Ganichev S D 1999 *Physica* B **273–274** 737
[27] Ganichev S D, Bel'kov V V, Golub L E, Ivchenko E L, Schneider P, Giglberger S, Eroms J, De Boeck J, Borghs G, Wegscheider W, Weiss D and Prettl W 2004 *Phys. Rev. Lett.* **92** 256601
[28] Ivchenko E L, Lyanda-Geller Yu B and Pikus G E 1988 *Ferroelectrics* **83** 19
[29] Ivchenko E L, Lyanda-Geller Yu B, Pikus G E and Rasulov R Ya 1984 *Fiz. Tekh. Poluprov.* **18** 93
Ivchenko E L, Lyanda-Geller Yu B, Pikus G E and Rasulov R Ya 1984 *Sov. Phys.—Semicond.* **18** 55 (Engl. Transl.)
[30] Ivchenko E L, Pikus G E and Rasulov R Ya 1984 *Fiz. Tverd. Tela* **26** 3362
Ivchenko E L, Pikus G E and Rasulov R Ya 1984 *Sov. Phys.—Solid State* **26** 2020 (Engl. Transl.)
[31] Astaf'ev S B, Lazarev V G, Lyanda-Geller Yu B and Fridkin V M 1988 *Fiz. Tverd. Tela* **30** 3362
Astaf'ev S B, Lazarev V G, Lyanda-Geller Yu B and Fridkin V M 1988 *Sov. Phys.—Solid State* **30** 1932 (Engl. Transl.)
[32] Andrianov A V, Beregulin E V, Lyanda-Geller Yu B and Yaroshetskii I D 1992 *Zh. Eksp. Teor. Fiz.* **102** 1703
Andrianov A V, Beregulin E V, Lyanda-Geller Yu B and Yaroshetskii I D 1992 *JETP* **75** 921 (Engl. Transl.)
[33] Ivchenko E L and Pikus G E 1997 *Superlattices and Other Heterostructures. Symmetry and Optical Phenomena* (Berlin: Springer)
[34] Sturman B I and Fridkin V M 1992 *The Photovoltaic and Photorefractive Effects in Non-Centrosymmetric Materials* (Philadelphia, PA: Gordon and Breach)
[35] Magarill L I, Palkin A M, Sozinov V N and Entin V M 1990 *Zh. Eksp. Teor. Fiz.* **97** 950
Magarill L I, Palkin A M, Sozinov V N and Entin V M 1990 *JETP* **70** 533 (Engl. Transl.)
[36] Stern F and Howard W E 1967 *Phys. Rev.* **163** 816
[37] Ando T 1978 *J. Phys. Soc. Japan* **44** 475
[38] Ando T, Fowler A B and Stern F 1982 *Rev. Mod. Phys.* **54** 437
[39] Crasemann J H, Merkt U and Kotthaus J P 1983 *Phys. Rev.* B **28** 2271
[40] Zawadzki W, Klahn S and Merkt U 1986 *Phys. Rev.* B **33** 6916
[41] Heisz J M and Zaremba E 1993 *Semicond. Sci. Technol.* **8** 575
[42] Ivchenko E L and Tarasenko S A 2004 *Zh. Eksp. Teor. Fiz.* **126** 476
Ivchenko E L and Tarasenko S A 2004 *JETP* **99** 379 (Engl. Transl.)
[43] Belinicher V I 1982 *Fiz. Tverd. Tela* **24** 15
Belinicher V I 1982 *Sov. Phys.—Solid State* **24** 7 (Engl. Transl.)
[44] Averkiev N S, Golub L E and Willander M 2002 *J. Phys.: Condens. Matter* **14** R271
[45] Tarasenko S A and Ivchenko E L 2005 *Pis. Zh. Eksp. Teor. Fiz.* **81** 292
Tarasenko S A and Ivchenko E L 2005 *JETP Lett.* **81** 231 (Engl. Transl.)
[46] Ganichev S D, Schneider P, Bel'kov V V, Ivchenko E L, Tarasenko S A, Wegscheider W, Weiss D, Schuh D, Clarke D G, Merrick M, Murdin B N, Murzyn P, Phillips P J, Pidgeon C R, Beregulin E V and Prettl W 2003 *Phys. Rev.* B **68** 081302 (Rapid Communication)
[47] Ivchenko E L and Pikus G E 1980 *Problemy Sovremennoi Fiziki* (Leningrad: Nauka) pp 275–93
Ivchenko E L and Pikus G E 1986 *Semiconductor Physics* (New York: Plenum) pp 427–47 (Engl. Transl.)